

NJC

Accepted Manuscript



This is an *Accepted Manuscript*, which has been through the Royal Society of Chemistry peer review process and has been accepted for publication.

Accepted Manuscripts are published online shortly after acceptance, before technical editing, formatting and proof reading. Using this free service, authors can make their results available to the community, in citable form, before we publish the edited article. We will replace this *Accepted Manuscript* with the edited and formatted *Advance Article* as soon as it is available.

You can find more information about *Accepted Manuscripts* in the [Information for Authors](#).

Please note that technical editing may introduce minor changes to the text and/or graphics, which may alter content. The journal's standard [Terms & Conditions](#) and the [Ethical guidelines](#) still apply. In no event shall the Royal Society of Chemistry be held responsible for any errors or omissions in this *Accepted Manuscript* or any consequences arising from the use of any information it contains.

Cite this: DOI: 10.1039/c0xx00000x

www.rsc.org/xxxxxx

ARTICLE TYPE

Tuning the magnetic, oxidation state and coordination behaviour of Iron and Cobalt Complexes on O/S variation in mono-thio and dithio-oxamide chelating ligands

Luca Pilia,^{*a} Davide Espa,^b Giorgio Concas,^c Francesco Congiu,^c Luciano Marchiò,^d M. Laura Mercuri,^b Angela Serpe^b and Paola Deplano^{*b,c}

Received (in XXX, XXX) Xth XXXXXXXXXX 20XX, Accepted Xth XXXXXXXXXX 20XX

DOI: 10.1039/b000000x

New iron and cobalt complexes coordinated with the ligands Me₂pipto (*N,N'*-dimethyl-piperazine-3-oxo-2-thione) and Me₂pipdt (*N,N'*-dimethyl-piperazine-2,3-dithione, S,S') differing for one sulphur substituting the oxygen atom, have been prepared and characterized. The reaction with Me₂pipto and iron salts affords the heteroleptic [Fe^{III}(Me₂pipto)₂Cl₂]⁺ or the homoleptic [Fe^{II}(Me₂pipto)₃]²⁺ cationic complexes (isolated as tetrafluoroborate salts **1** and **2**) depending on the employed iron source: FeCl₃ or Fe₂(SO₄)₃ respectively. The corresponding reaction with CoCl₂ as metal source allowed to obtain [Co^{II}(Me₂pipto)₃](BF₄)₂ (**3**). By reacting FeCl₃, Me₂pipto and KSCN in the molar ratios 1:1:4, [Fe^{III}(Me₂pipto)(NCS)₄]⁻ is obtained and isolated as Ph₄P⁺ salt (**4**). By using Me₂pipdt ligand, the reaction with FeCl₃ affords [Fe^{II}(Me₂pipdt)₃]²⁺ which is isolated as tetrafluoroborate salt (**5**). The same cation is found in the polyiodide salt [Fe^{II}(Me₂pipdt)₃](I₃)_{1.8}(I_{0.2}) (**6**) obtained by reacting iron-metal powders with Me₂pipdt and I₂ mixtures. Through a similar reaction by using cobalt-metal powders, [Co^{III}(Me₂pipdt)₃]₂(I₃)₂(I₄·2I₂) (**7**) is obtained. Structural results show that in all these compounds the metal ions are in a pseudo-octahedral coordination geometry and that bond distances are consistent with the presence of an iron(III) in **1** and **4** and with iron(II) in **2** and cobalt(III) in **7**. Magnetic susceptibility measurements, show that the metals are in a high spin state in all Me₂pipto complexes and a low spin state in Me₂pipdt ones. The observed differences are related to the different σ-donor and π-acceptor capabilities of the ligands tuned by the S and O donor atoms. Results from DFT calculations using B3LYP and OLYP as functionals are in agreement with the observed magnetic behaviour of complexes.

Introduction

The donor properties towards transition metals (acceptor) of the oxygen and sulphur chalcogen atoms show differences roughly related to their *hard* and *soft* character in accordance with the former Hard and Soft Acids and Bases (HSAB) Concept,¹ or more appropriately with the different extent of frontier orbitals donor/acceptor interactions. As well known, when compared with oxygen-donors, sulphur-ones possess larger atomic radius and increased size of the orbitals. When both O and S atoms are present in the same ligand a tuning of properties may be observed in their metal-complexes. As an interesting example it may be cited the reversible “redox-induced linkage isomerism” shown by the ambidentate ligand 2-methylisothiazol-3(2*H*)-one (MIO, see Chart 1) able to bond a variety of metals with either oxygen or a sulphur atom. It is found that MIO coordinates to the metal centers through its oxygen atom, in the cobalt(III), ruthenium(III), and uranium(VI) complexes but through its sulphur atom in the ruthenium(II) and platinum(III) complexes.²

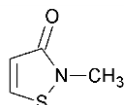


Chart 1

The prevailing hard/soft character when both O and S atoms are included in a bidentate chelating moiety is less predictable. Several bidentate chelate ligands bearing sulphur and/or oxygen donor atoms have been studied in the last decades.³ The coordinating properties of α-dithio-oxamides towards *soft-metals* have been exploited to add favourable conditions to oxidize crude metals in very mild conditions by employing their mixtures or adducts with diiodide.⁴ Moreover several Ni-triad mixed-ligand dithione-dithiolato complexes, based on R₂pipdt (*N,N'*-dialkyl-piperazine-2,3-dithione) and several dithiolate ligands, which behave as redox-active second order nonlinear optical chromophores,^{3e,6} have been prepared, and the electrodonating/withdrawing features of the ligands, the π-delocalization between them, and the *nd*-metal orbitals thoroughly investigated.^{6,7} Being interested to investigate the variation of the properties of these (S,S') chelating ligands by substituting one oxygen for one sulphur atom, the *N,N'*-dimethyl-piperazine-3-oxo-2-thione (Me₂pipto, S,O) ligand has been prepared and characterized.⁸ In agreement with experimental evidences, DFT calculations have shown that the energies of the LUMO and HOMO are, respectively, pitched up and down compared to the corresponding frontier orbitals of the R₂pipdt ligand. Energies and shape of these orbitals, suggest a greater capability of the S,S' ligand with respect to S,O one to work both as σ-donor (HOMO) and π-acceptor (LUMO) (see Figure S1).

Differences in the coordination properties between the two ligands have been displayed in the reaction of these donors with the Ni(II) ion (borderline acid): while the R₂pipdt ligand gives the diamagnetic square-planar [Ni(Me₂pipdt)₂]²⁺ complex^{5a}, as already reported, the S,O one produces, in the same conditions, the paramagnetic octahedral compound⁸ [Ni(Me₂pipto)₃]²⁺.

In this paper iron and cobalt, completing the first row 8a group and predictable hard as M(III) and borderline as M(II) ions, with these ligands are investigated. Accordingly the synthesis and characterization, including magnetic and single X-ray structural studies, of a variety of iron and cobalt complexes (1-7, Scheme 1, Results and Discussion below) coordinated with the ligands Me₂pipto and their comparison with those obtained with Me₂pipdt are reported. DFT calculations using B3LYP and OLYP as functionals are discussed to provide a reasonable explanation of the observed magnetic behaviour.

Experimental section

All the reagents and solvents were purchased from Aldrich and used without further purification. The Me₂pipdt^{5,9} and the Me₂pipto⁸ ligands were prepared as previously described.

Measurements

Elemental analyses were performed by means of a Carlo Erba CHNS Elemental Analyzer Model EA1108. Electronic spectra (900–200 nm) were recorded on a Cary 5 spectrophotometer in CH₃CN solutions. I.R. spectra (4000–400 cm⁻¹) were recorded with a Bruker IFS55 FT-IR Spectrometer on KBr pellets. FT-Raman spectra (resolution 4 cm⁻¹) were recorded on a Bruker RFS100 FT-spectrometer, fitted with an indium-gallium-arsenide detector (room temperature) and operating with an excitation frequency of 1064 nm (Nd:YAG laser). The power level of the laser source varied between 20 and 40 mW. The solid samples were introduced in a capillary tube and then fitted into the compartment designed for a 180° scattering geometry.

Preparation

[Fe(Me₂pipto)₂Cl₂](BF₄) (1). *Synthesis:* 474.2 mg (3.0 mmol) of Me₂pipto in 60 mL of CH₃CN, yellow solution, were added drop-wise to a solution of FeCl₃ (243.3 mg, 1.5 mmol) in the same solvent (150 mL); the solution became red-orange. After the addition of 210 mg of NaBF₄ (1.9 mmol) and 1 hour of stirring, the solvent was evaporated and the crude product dissolved with CH₃CN (30 mL) and filtered to separate a white solid. An orange solid was obtained by a drop-wise addition of diethyl ether; the precipitate was collected by filtration and washed with diethyl ether (three times)(yield 360.2 mg, 0.68mmol; 45.5%). The same compound has been obtained using a 3:1 (Me₂pipto: FeCl₃) molar ratio. Analytical results are in accordance with the formula [Fe(Me₂pipto)₂Cl₂](BF₄). *Elemental Analysis:* calculated for C₁₂H₂₀N₄O₂S₂Cl₂FeBF₄ (529.99): C 27.20, H 3.80, N 10.57, S 12.10; found: C 26.96, H 3.41, N 10.52, S 12.30. *UV-vis* (in CH₃CN solution): λ/nm (ε/mol·cm⁻¹·dm⁻³) 480 (sh); 320 (2.37·10⁴); 274 (2.18·10⁴). *FT-IR* (KBr): ν_{max}/cm⁻¹ 3000w; 2928w; 2855w; 1657vs (νCO); 1637s 1573vs (νCN); 1540mw; 1521w; 1505w; 1474m; 1455m; 1439m; 1406ms; 1369ms; 1352m; 1257m; 1206m; 1161m; 1100ms; 1083ms; 1056s; 958w; 895mw; 830vw; 753m; 698m; 667w; 583m; 560w; 520vw;

500vw; 440m.

[Fe(Me₂pipto)₃](BF₄)₂ (2). *Synthesis:* 316.0 mg (2.0 mmol) of 1 in 40 ml of CH₃CN, yellow solution, was added drop-wise to a suspension of Fe₂(SO₄)₃·xH₂O (133.0 mg, 0.34 mmol) in the same solvent (50 ml); after adding few drops of H₂SO₄ 96% the solution turned orange. After the addition of 240 mg of NaBF₄ (2.2 mmol) the solution turned red-violet during the stirring at reflux (3 h). The solvent was evaporated and the crude product dissolved with CH₃CN (60 ml). This solution was filtered to separate a white solid, and Na₂SO₄ was added to remove water. The addition of THF caused the formation of a white precipitate that was removed before a drop-wise addition of diethyl ether; the formed lacquer, became slowly a crystalline solid that was recrystallized from acetone/Et₂O; the precipitate was collected by filtration and washed with diethyl ether (three times) (yield 55.4 mg, 0.078 mmol; 23.4%). Analytical results are in accordance with the formula [Fe(Me₂pipto)₃](BF₄)₂. *Elemental Analysis:* calculated for C₁₈H₃₀N₆O₃S₃FeB₂F₈ (704.11): C 30.70, H 4.29, N 11.94, S 13.66; found: C 31.00, H 3.91, N 11.94, S 13.30. *UV-vis* (in CH₃CN solution): λ/nm (ε/mol·cm⁻¹·dm⁻³) 530 (400); 430 (500); 310 (1.73·10⁴); 270 (1.63·10⁴). *FT-IR* (KBr): ν_{max}/cm⁻¹ 293w; 2859vw; 1639vs (νCO); 1558vs (νCN); 1507w; 1489w; 1439w; 1404mw; 1369m; 1262w; 1208mw; 1160w; 1083(ms); 1054s; 961w; 896w; 830vw; 755w; 695w; 668vw; 584mw; 521w; 501vw; 418m.

[Co(Me₂pipto)₃](BF₄)₂ (3). *Synthesis:* 105.3 mg (0.66 mmol) of Me₂pipto in 20 mL of CH₃CN were added drop-wise to a solution of CoCl₂·6H₂O (52.35 mg, 0.22 mmol) in the same solvent (25 mL); after the addition of 48.3 mg of NaBF₄ (0.44 mmol) the mixture has been stirred for 5 h at room temperature, then the solvent was evaporated and the obtained light brown solid dissolved with acetonitrile and filtered (a white solid has been separated). The solution has been treated with Na₂SO₄ anhydrous and, after filtration, diethyl ether was added and a light brown solid appeared. This solid has been collected by centrifugation and washed three times with diethyl ether (yield 94.0 mg, 0.13mmol; 59.1%). Analytical results are in accordance with the formula [Co(Me₂pipto)₃](BF₄)₂. *Elemental Analysis:* calculated for C₁₈H₃₀N₆O₃S₃CoB₂F₈ (707.21): C 30.57, H 4.28, N 11.88, S 13.60; found: C 30.85, H 4.42, N 11.78, S 13.60. *UV-vis* (in CH₃CN solution): λ/nm (ε/mol·cm⁻¹·dm⁻³) 310 (1.98·10⁴); 280 (1.92·10⁴). *FT-IR* (KBr): ν_{max}/cm⁻¹ 2973vw; 2930w; 2863vw; 1644vs (νCO); 1557vs (νCN); 1488mw; 1438mw; 1406m; 1367ms; 1264m; 1208m; 1159ms; 1106s; 1083s; 1028s; 961mw; 899mw; 835vw; 756mw; 698mw; 582mw; 534w; 522w; 493w.

Ph₄P[Fe(Me₂pipto)(NCS)₄] (4). *Synthesis:* 100.0 mg (0.63 mmol) of Me₂pipto in 10 mL of CH₃CN, have been added drop-wise to a solution of FeCl₃ (102.5 mg, 0.63 mmol) in the same solvent (40 mL) followed by a solution of 245.5 mg of KSCN (2.53 mmol) in 30 mL of CH₃CN. After the addition of 264.2 mg of tetraphenylphosphonium bromide (0.63 mmol) in 20 mL of CH₃CN, diethyl ether has been added until the formation of a white solid which has been separated by filtration. A further addition of Et₂O produced a brown solid which has been collected by filtration and recrystallized from CH₃CN/Et₂O (yield 360.0 mg, 0.458mmol; 72.7%). Analytical results are in accordance with the formula Ph₄P[Fe(Me₂pipto)(NCS)₄]. *Elemental Analysis:* calculated for C₃₄H₃₀N₆O₅FeP (785.79): C

51.97, H 3.85, N 10.70, S 20.40; found: C 51.16, H 3.44, N 10.56, S 20.30. *UV-vis* (in CH₃CN solution): λ /nm (ϵ /mol·cm⁻¹·dm⁻³) 502 (1.40·10⁴); 300 (9.40·10³). *FT-IR* (KBr): ν_{max} /cm⁻¹ 3055vw; 3018vw; 2922w; 2859vw; 2076s; 2036vs; 1638s (vCO); 1553ms (vCN); 1479mw; 1437ms; 1401mw; 1368m; 1314vw; 1254w; 1204mw; 1160mw; 1110s; 996w; 900w; 842w; 753m; 720s; 690s; 584w; 527s; 481mw; 447mw.

[Fe(Me₂pipdt)₃](BF₄)₂ (5). *Synthesis:* 322.0 mg (1.84 mmol) of Me₂pipdt in 50 mL of acetone, red-brown solution, were added drop-wise to a solution of FeCl₃ (100.0 mg, 0.61 mmol) in acetone (30 mL). The solvent was evaporated and a green-brown solid obtained; the green product was dissolved with methanol and separated by filtration from a brown solid. 140.0 mg of NaBF₄ (1.28 mmol) in 40 mL of MeOH were added to the solution and a crystalline green solid appeared. The solid has been collected by filtration and washed three times with diethyl ether (yield 322.1 mg, 0.42 mmol; 70.2%). Analytical results are in accordance with the formula [Fe(Me₂pipdt)₃](BF₄)₂. *Elemental Analysis:* calculated for C₁₈H₃₀N₆S₆FeB₂F₈ (752.29): C 28.74, H 4.02, N 11.17, S 25.27; found: C 28.94, H 4.23, N 11.18, S 25.02. *UV-vis* (in CH₃CN solution): λ /nm (ϵ /mol·cm⁻¹·dm⁻³) 873 (4.40·10³); 788 (4.26·10³); 340 (1.27·10⁴); 240 (sh). *FT-IR* (KBr): ν_{max} /cm⁻¹ 2950vw; 2854vw; 1528vs (vCN); 1457mw; 1397ms; 1354vs; 1286w; 1261m; 1205w; 1083s; 1057s; 818vw; 671w; 522w; 456w; 421w.

[Fe(Me₂pipdt)₃](I₃)_{1.8}(I)_{0.2} (6). I₂ (72.82 mg, 0.29 mmol) was added to Me₂pipdt (50.00 mg; 0.28 mmol) and Fe as metal powder (53.40 mg; 0.96 mmol) in THF (50 mL). The solution was left under reflux for 24 h. The solvent was rotary-evaporated and the crude product dissolved in MeOH. The unreacted reagents were removed by filtration. The brown product was collected by filtration and recrystallized by MeOH/CH₃CN (71.60 mg, 0.056 mmol, yield 60%). *Elemental Analysis:* calculated for C₁₈H₃₀N₆FeS₆I_{5.6} (1289.35): C 16.77, H 2.34, N 6.52, S 15.92; found: C 16.90, H 2.21, N 6.48, S 15.36. *UV-vis* (in CH₃CN solution): λ /nm (ϵ /mol·cm⁻¹·dm⁻³) 862 (2.83·10³); 788 (2.72·10³); 360 (4.20·10⁴); 287 (1.15·10⁵). *FT-IR* (KBr): ν_{max} /cm⁻¹ 1520vs (vCN); 1450w; 1410m; 1350vs; 1260m; 1210w; 1150w; 1110w; 1040w; 1020w; 910w; 880w; 820w; 670w; 550w.

[Co^{III}(Me₂pipdt)₃](I₃)₂(I)₄·2I₂ (7). I₂ (72.82 mg, 0.29 mmol) was added to Me₂pipdt (50.00 mg; 0.28 mmol) and Co as metal powder (56.36 mg; 0.96 mmol) in THF (50 mL). The solution was left under reflux for 24 h. The solvent was rotary-evaporated and the crude product dissolved in MeOH. The unreacted reagents were removed by filtration. The crude red brown product was collected by filtration and recrystallized by MeOH/CH₃CN (79.00 mg, 0.054 mmol, yield 65%). *Elemental Analysis:* calculated for C₁₈H₃₀N₆CoS₆I₇ (1470.13): C 14.71, H 2.06, N, 5.72, S 13.09; found: C 14.84, H 1.90, N 5.76, S 13.32. *UV-vis* (in CH₃CN solution): λ /nm (ϵ /mol·cm⁻¹·dm⁻³) 495 (sh); 361 (7.55·10⁴); 292 (1.29·10⁵); 246 (sh); 210 (5.46·10⁴). *FT-IR* (KBr): ν_{max} /cm⁻¹ 1548vs (vCN); 1440w; 1400w; 1360s; 1290m; 1270m; 1150m; 1110w; 1030w; 900w; 550w. *FT-Raman:* ν_{max} /cm⁻¹ 147m; 108vs.

55 X-ray crystallography

A summary of data collection and structure refinement for [Fe(Me₂pipto)₂Cl₂](BF₄) (1), Ph₄P[Fe(Me₂pipto)(NCS)₄] (4), [Fe(Me₂pipdt)₃](BF₄)₂ (5), [Fe(Me₂pipdt)₃](I₃)_{1.8}(I)_{0.2} (6) and

[Co(Me₂pipdt)₃](I₃)₂(I)₄·2I₂ (7) are reported in Table 1. Single crystal data were collected with a Bruker AXS Smart 1000 CCD (1 and 6), with a Philips PW 1100 (4 and 5) and with a Bruker Smart Breeze CCD (7). All data collection were performed with the Mo K α radiation (λ = 0.71073 Å). Cell constants of 4 and 5 were obtained by a least-square refinement of the setting angles of 24 randomly distributed and carefully centered reflections, whereas the unit cell parameters of 1, 6 and 7 were obtained using 60 ω -frames of 0.5° width and scanned from three different zone of reciprocal lattice. The intensity data of 1 and 7 were integrated from several series of exposures frames (0.3° width) covering the sphere of reciprocal space, whereas the crystals of 6 slowly decomposed during the data collection and only a limited number of frames could be collected affording a data completeness of approximately 75%.¹⁰ Absorption corrections were applied using the program NEWABS92¹¹ (4 and 5, with min. and max. transmission factors of 0.894-1.000 for 4 and 0.944-1.000 for 5), and the program SADABS¹² (1, 6 and 7, with min. and max. transmission factors of 0.802-1.000 for 1, 0.457-1.000 for 6 and 0.373-1.000 for 7). The structures were solved by direct methods (SIR97¹³ and SIR2004¹⁴) and refined on F^2 with full-matrix least squares (SHELXL-97¹⁵), using the Wingx software package.¹⁶ In 5 the BF₄⁻ anion was found disordered in three position that were each refined with site occupancy factors (s.o.f.) of 0.33. These three fractions of BF₄⁻ were refined with isotropic thermal parameters. The complex molecule of 5 lied on two-fold crystallographic axis and one of the ligands was disordered in two positions with s.o.f. of 0.5. In 1 the BF₄⁻ anion was found disordered in two positions with s.o.f. of 0.63/0.37. In 6 one of the I₃⁻ anion was found disordered in two positions, which occupy a channel like cavity. In 7 the iodine atoms showed a severe disorder concerning the various forms in which it is present in the structure. In particular, one of the I₃⁻ anion was disordered in two positions whereas a second I₃⁻ anion was found disordered in various positions, which occupy a channel like cavity. In order to support the iodine content in the molecular structures of 6 and 7, the SQUEEZE procedure was applied on the structural models devoid of the iodine fragments disordered in channel-like cavities. In 6, these iodine fragments were assigned to 5.2 iodine atoms, which amount to 276 electrons/unit cell. This is in agreement with the computed 340 electrons/unit cell. In 7, the disordered iodine fragments in the channels were assigned to 12 iodine atoms, corresponding to 758 electrons/unit cell, in agreement with the computed 736 electrons/unit cell. For all structures the hydrogen atoms were placed at their calculated positions during the refinement. Graphical material was prepared with the ORTEP3 for Windows¹⁶ and Mercury CSD 3.0¹⁷ programs. CCDC 1037915-1037919 contain the supplementary crystallographic data for this paper.

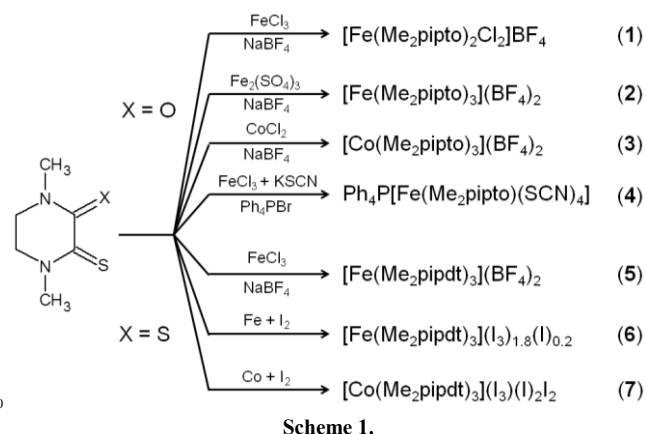
Theoretical calculations

Ground-state electronic structure calculations of complexes 1 and 3 have been performed at Density Functional Theory (DFT)¹⁸ level employing the GAUSSIAN 09¹⁹ software packages. The functional used was B3LYP^{20, 21} with the basis set 6-31G(d)^{22, 23} employed for all atoms. The ground state geometries were obtained in the gas phase, by full geometry optimization without any symmetry constrain, starting from the structural data with the exception of complex 3. In order to evaluate the difference in

energy between the high (HS) and low spin (LS) configurations, in addition to those with B3LYP, calculations employing the pure density functional OLYP²⁴ and the basis set 6-31G(d), have been done for the complexes **1** and **3**. In the case of **1**, the geometries were optimized for both, HS and LS, starting from the X-ray structure, while the structure of **3** was input through ArgusLab 4.0 program.²⁵ Single point calculations have been performed with both the functionals mentioned above and with the basis set 6-311+G(d,p).^{26, 27} The optimized molecular structures were visualized using ArgusLab 4.0.²⁵

Magnetic Measurements

The DC magnetic susceptibility of compounds **1-5** and **7** were measured using a SQUID magnetometer (Quantum Design MPMS-XL 5T). The samples in powder form were embedded in a teflon tape and the susceptibility of Teflon was measured and subtracted; the susceptibility data were corrected for the diamagnetic contributions of the salt. The susceptibility was measured in CGS units in the temperature range 2-400 K with an applied field of 10 kG.



Results and Discussion

As shown in Scheme 1, the reaction with Me₂pipto and iron salts affords the heteroleptic [Fe^{III}(Me₂pipto)₂Cl₂]⁺ or the homoleptic [Fe^{III}(Me₂pipto)₃]²⁺ cationic complexes (isolated as tetrafluoroborate salts **1** and **2**) depending on the employed iron source: FeCl₃ or Fe₂(SO₄)₃ respectively. The corresponding reaction with CoCl₂ as metal source allowed to obtain [Co^{II}(Me₂pipto)₃](BF₄)₂ (**3**). By reacting FeCl₃, Me₂pipto and KSCN in the molar ratios 1:1:4, [Fe^{III}(Me₂pipto)(NCS)₄]⁻ is obtained and isolated as Ph₄P⁺ salt (**4**). By using Me₂pipdt ligand, the reaction with FeCl₃ affords [Fe^{II}(Me₂pipdt)₃]²⁺ which is isolated as tetrafluoroborate salt (**5**). The same cation is found in the polyiodide salt [Fe^{II}(Me₂pipdt)₃](I₃)_{1.8}(I)_{0.2} (**6**) obtained by reacting iron-metal powders with Me₂pipdt and I₂ mixtures. Through a similar reaction by using cobalt-metal powders, [Co^{III}(Me₂pipdt)₃](I₃)(I)₂ (**7**) is obtained. The molecular structures of the complexes [Fe(Me₂pipto)₂Cl₂](BF₄) (**1**), Ph₄P[Fe(Me₂pipto)(NCS)₄] (**4**), [Fe(Me₂pipdt)₃](BF₄)₂ (**5**), [Fe(Me₂pipdt)₃](I₃)_{1.8}(I)_{0.2} (**6**) and [Co^{III}(Me₂pipdt)₃](I₃)₂(I)₄·2I₂ (**7**), are reported in Figures 1-5. In all compounds, the metal is in

an pseudo-octahedral geometry. In **1**, the metal is surrounded by two chlorine atoms and by two oxygen atoms in *cis* position, and by two sulphur atoms in *trans* position. The metal is in the 3+ oxidation state and the charge is balanced by the presence of a BF₄⁻ anion *per* each complex molecule; the two Me₂pipto ligands act in the S,O bidentate mode. In **4**, the metal is bound by four nitrogen atoms of the thiocyanate ligands that are arranged in a seesaw geometry. The presence of the Me₂pipto ligand completes the octahedral coordination of iron. The metal is in the 3+ oxidation state and the overall negative charge of the complex is balanced by a PPh₄⁺ cation. In **5** and **6**, the metal is in the 2+ oxidation state in agreement with the presence of three *softer* S,S' bidentate Me₂pipdt ligands, whose bite angles, close to 90°, lead to the formation of a nearly regular coordination environment. As far as the metal-sulphur bond distances are concerned, in **1** and **4** they are, on average, 0.2 Å longer than those found in **5** and **6** (2.314(1)–2.279(2) Å in **5** and 2.305(5)–2.258(6) Å in **6**) and of the Fe-Cl distances (Tables 2 and 3).

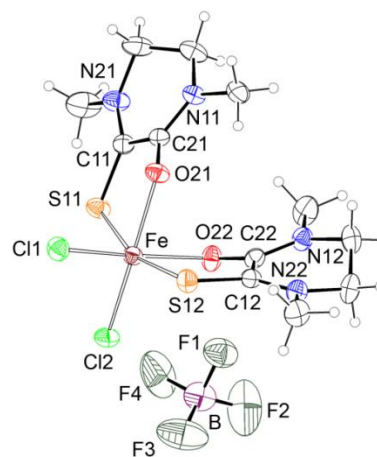


Figure 1. Ortep diagram of [Fe(Me₂pipto)₂Cl₂](BF₄) (**1**) with thermal ellipsoids drawn at the 30% probability level.

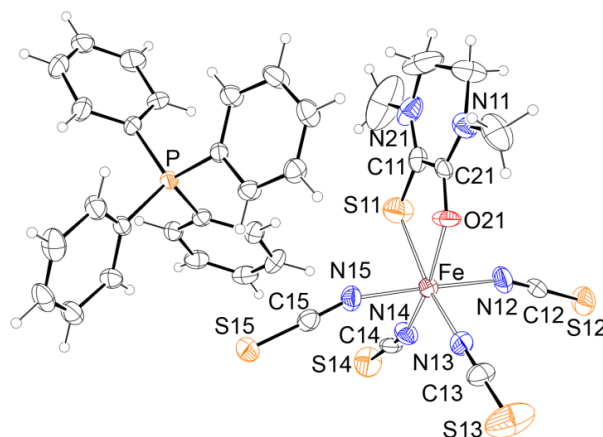


Figure 2. Ortep diagram of Ph₄P[Fe(Me₂pipto)(NCS)₄] (**4**) with thermal ellipsoids drawn at the 30% probability level.

Table 1. Summary of X-ray crystallographic data for [Fe(Me₂pipto)₂Cl₂](BF₄) (1), Ph₃P[Fe(Me₂pipto)(NCS)₄] (4), [Fe(Me₂pipdt)₃](BF₄)₂ (5), [Fe(Me₂pipdt)₃](I₃)_{1.8}(I_{0.2}) (6) and [Co(Me₂pipdt)₃](I₃)₂(I₄)₂I₂ (7).

	1	4	5	6	7
Empirical formula	C ₁₂ H ₂₀ Cl ₂ F ₄ FeN ₄ O ₂ S ₂	C ₃₄ H ₃₀ FeN ₆ OPS ₅	C ₁₈ H ₃₀ B ₂ F ₈ FeN ₆ S ₆	C ₁₈ H ₃₀ FeI _{5.6} N ₆ S ₆	C ₃₆ H ₆₀ Co ₂ I ₄ N ₁₂ S ₁₂
Formula weight	530.00	785.76	752.31	1289.33	2940.14
Crystal system	Monoclinic	Monoclinic	Monoclinic	Triclinic	Monoclinic
Space group	<i>P</i> 2 ₁ / <i>c</i>	<i>Cc</i>	<i>C</i> 2/ <i>c</i>	<i>P</i> -1	<i>C</i> 2/ <i>c</i>
<i>a</i> , Å	9.978(1)	9.59(1)	22.662(5)	8.487(4)	14.543(1)
<i>b</i> , Å	12.495(1)	31.06(2)	11.130(3)	13.970(6)	42.417(3)
<i>c</i> , Å	17.672(2)	12.91(2)	18.004(4)	16.988(9)	14.520(1)
α, deg.	90	90	90	73.85(1)	90
β, deg.	97.174(5)	97.82(3)	134.54(2)	77.69(2)	115.476(1)
γ, deg.	90	90	90	76.69(2)	90
<i>V</i> , Å ³	2186.0(4)	3810(8)	3237(1)	1859(2)	8086(1)
<i>Z</i>	4	4	4	2	4
<i>T</i> , K	293(2)	293(2)	293(2)	293(2)	293(2)
ρ (calc), Mg/m ³	1.610	1.370	1.544	2.304	2.415
μ, mm ⁻¹	1.174	0.748	0.921	5.414	6.100
θ range, deg.	2.00 to 27.51	3.07 to 27.01	3.07 to 26.00	2.22 to 24.04	0.96 to 26.60
No. of rflcn/unique	23266 / 4893	4292 / 4292	3258 / 3160	5289 / 4449	49411 / 8379
Goof	1.004	1.007	0.974	1.021	1.043
<i>R</i> 1	0.0331	0.0563	0.0482	0.0796	0.0596
<i>wR</i> 2	0.0860	0.1305	0.0592	0.1780	0.1780

$$R1 = \frac{\sum ||F_o| - |F_c||}{\sum |F_o|}, wR2 = \frac{[\sum [w(F_o^2 - F_c^2)^2] / \sum [w(F_o^2)^2]]^{1/2}}{w}, w = 1/[\sigma^2(F_o^2) + (aP)^2 + bP], \text{ where } P = [\max(F_o^2, 0) + 2F_c^2] / 3$$

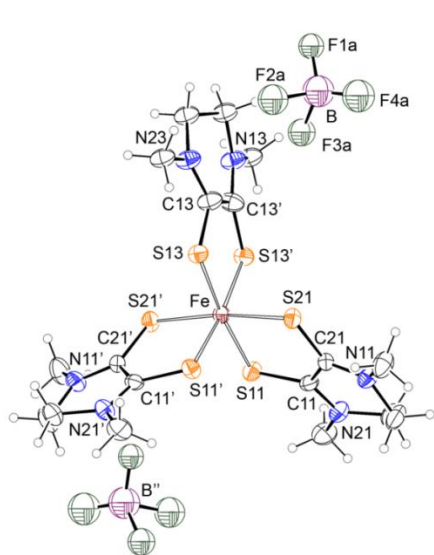


Figure 3. Ortep diagram of [Fe(Me₂pipdt)₃](BF₄)₂ (5) with thermal ellipsoids drawn at the 30% probability level. Symmetry codes ' = 1-x, y, 1/2-z; '' = 1-x, y-1, 1/2-z.

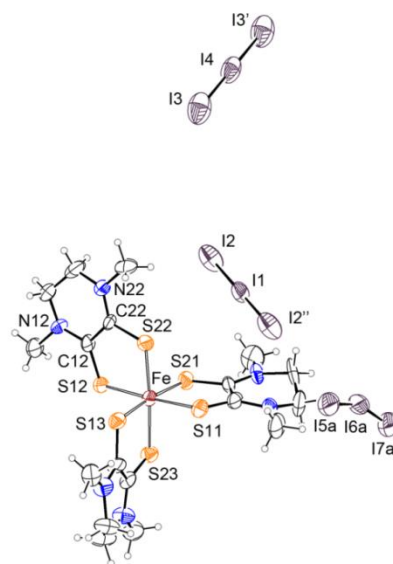


Figure 4. Ortep diagram of [Fe(Me₂pipdt)₃](I₃)_{1.8}(I_{0.2}) (6) with thermal ellipsoids drawn at the 30% probability level. Symmetry codes: ' = 1-x; 1-y; 2-z; '' = 1-x; 1-y; 1-z.

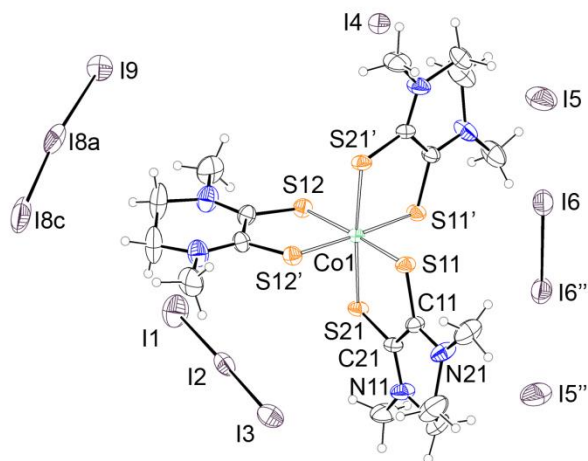


Figure 5. Ortep diagram of $[\text{Co}(\text{Me}_2\text{pipdt})_3]_2(\text{I}_3)_2(\text{I})_4 \cdot 2\text{I}_2$ (**7**) with thermal ellipsoids drawn at the 30% probability level. Only one complex molecules comprising the asymmetric unit is reported for clarity.

Symmetry codes: ' = $x, -y, z+1/2$, '' = $-x, y, 1/2-z$.

Table 2. Selected bond lengths (Å) and angles (°) for **1** and **4**.

1			
Fe-S(11)	2.5022(7)	S(11)-Fe-O(22)	89.35(5)
Fe-S(12)	2.4595(6)	S(11)-Fe-O(21)	78.13(4)
Fe-O(21)	2.101(1)	S(11)-Fe-Cl(2)	88.26(2)
Fe-O(22)	2.071(2)	S(11)-Fe-Cl(1)	101.78(3)
Fe-Cl(1)	2.2699(7)	S(12)-Fe-O(22)	80.08(4)
Fe-Cl(2)	2.2592(6)	S(12)-Fe-O(21)	87.37(4)
C(11)-S(11)	1.675(2)	S(12)-Fe-Cl(2)	105.15(3)
C(21)-O(21)	1.248(2)	S(21)-Fe-Cl(1)	87.13(2)
C(12)-S(12)	1.679(2)	O(22)-Fe-Cl(2)	93.53(5)
C(22)-O(22)	1.258(2)	O(21)-Fe-Cl(1)	93.23(5)
C(11)-C(21)	1.510(3)	O(21)-Fe-O(22)	80.72(6)
C(12)-C(22)	1.508(3)	Cl(1)-Fe-Cl(2)	95.19(2)
4			
Fe-S(11)	2.504(4)	C(15)-S(15)	1.621(9)
Fe-O(21)	2.145(6)	O(21)-Fe-S(11)	79.5(2)
Fe-N(12)	2.028(7)	N(14)-Fe-S(11)	86.3(3)
Fe-N(13)	2.035(8)	N(15)-Fe-S(11)	92.0(2)
Fe-N(14)	2.003(8)	N(12)-Fe-S(11)	88.2(2)
Fe-N(15)	2.007(7)	N(15)-Fe-O(21)	93.2(2)
C(11)-S(11)	1.603(9)	N(12)-Fe-O(21)	89.8(3)
C(21)-O(21)	1.300(9)	N(13)-Fe-O(21)	90.1(3)
C(11)-C(21)	1.50(1)	N(12)-Fe-N(13)	89.1(3)
C(12)-S(12)	1.615(9)	N(14)-Fe-N(12)	89.4(3)
C(13)-S(13)	1.60(1)	N(14)-Fe-N(15)	87.6(3)
C(14)-S(14)	1.64(1)	N(15)-Fe-N(13)	91.2(3)

Table 3. Selected bond lengths (Å) and angles (°) for **5** and **7**.

5			
Fe-S(11)	2.290(2)	C(13)-C(13)'	1.52(1)
Fe-S(21)	2.314(1)	S(11)-Fe-S(21)	90.18(7)
Fe-S(13)	2.279(2)	S(13)-Fe-S(13)'	88.5(1)
C(11)-S(11)	1.701(6)	S(11)-Fe-S(11)'	96.5(1)
C(21)-S(21)	1.681(6)	S(11)-Fe-S(21)'	84.89(7)
C(13)-S(13)	1.689(5)	S(21)-Fe-S(13)	85.96(7)
C(11)-C(21)	1.529(7)	S(21)-Fe-S(13)'	99.38(7)
6			
Fe-S(11)	2.251(5)	C(13)-C(23)	1.44(2)
Fe-S(21)	2.256(6)	S(22)-Fe-S(12)	88.0(2)
Fe-S(12)	2.243(4)	S(12)-Fe-S(23)	89.3(2)
Fe-S(22)	2.230(5)	S(22)-Fe-S(11)	90.1(2)
Fe-S(13)	2.258(5)	S(23)-Fe-S(11)	92.8(2)
Fe-S(23)	2.250(5)	S(22)-Fe-S(21)	94.1(2)
C(11)-S(11)	1.64(2)	S(12)-Fe-S(21)	90.0(2)
C(21)-S(21)	1.67(2)	S(23)-Fe-S(21)	89.2(2)
C(12)-S(12)	1.67(2)	S(11)-Fe-S(21)	87.5(2)
C(22)-S(22)	1.70(1)	S(22)-Fe-S(13)	90.2(2)
C(13)-S(13)	1.70(2)	S(12)-Fe-S(13)	94.9(2)
C(23)-S(23)	1.66(2)	S(23)-Fe-S(13)	86.8(2)
C(11)-C(21)	1.53(2)	S(11)-Fe-S(13)	87.7(2)
C(12)-C(22)	1.50(2)		
7			
Co(1)-S(11)	2.226(2)	S(11)-Co(1)-S(11)''	95.2(1)
Co(1)-S(21)	2.236(2)	S(11)-Co(1)-S(21)''	86.71(7)
Co(1)-S(12)	2.239(2)	S(11)-Co(1)-S(21)	89.55(7)
Co(2)-S(23)	2.230(2)	S(11)-Co(1)-S(12)''	87.79(7)
Co(2)-S(14)	2.231(2)	S(21)-Co(1)-S(12)''	94.16(7)
Co(2)-S(13)	2.242(2)	S(21)-Co(1)-S(12)	89.79(7)
S(21)-C(21)	1.683(7)	S(12)-Co(1)-S(12)''	89.2(1)
S(11)-C(11)	1.684(7)	S(14)-Co(2)-S(23)''	90.13(8)
S(12)-C(12)	1.670(7)	S(14)-Co(2)-S(23)	92.09(8)
S(13)-C(13)	1.671(8)	S(14)-Co(2)-S(14)''	89.5(1)
S(14)-C(14)	1.692(8)	S(13)-Co(2)-S(23)''	88.27(7)
S(23)-C(23)	1.696(8)	S(13)-Co(2)-S(23)	89.65(7)
C(11)-C(21)	1.488(9)	S(13)-Co(2)-S(14)	87.27(7)
C(23)-C(13)	1.49(1)	S(13)-Co(2)-S(13)''	95.9(1)

' = $1-x, y, 1/2-z$; '' = $-x, y, -z-1/2$

The smaller bite angle of Me_2pipto ($\approx 80^\circ$) implies that **1** and **4** exhibit a greater distortion from the ideal geometry when compared to **5** and **6**. The molecular structure of **7** comprises two cobalt(III) complexes, which exhibit the same octahedral geometry achieved by the coordination of three $\text{S}_2\text{S}'$ bidentate

Me₂pipdt ligands analogously to the structure of **5**. The metal-sulphur bond distances in **7** (range 2.226(2)–2.242(2) Å) are significantly shorter than those found for **5** in agreement with the small ionic radius of Co(III) with respect to Fe(II). Crystal packing motifs of **1**, **4**, **5**, **6** and **7** are shown in Figures S2–S6. In **7** the anions are represented by I[−] and I₃[−] species that together with the presence of I₂ surround the cobalt complexes. Interestingly, the I₂ moiety, I(6)–I(6)' exchange two weak interactions with two I[−] anions, I(5), which is located at 3.48 Å from I(6). The I₃[−] moieties comprising the I(8) and I(9) atoms is severely disordered and the linear molecular entity occupies a channel like cavity within the structure (Figure S6). This a structural feature that is also present in compound **6** (Figure S5). In all complexes, the C–C bond distance between the thioamido groups of Me₂pipdt and the thiamido and amido groups of Me₂pipto is approximately 1.5 Å,

in agreement with a single bond character. According to the coordination bond distances (Tables 2 and 3), **1** and **4** are in a high-spin state whereas, **5**, **6** and **7** are in a low-spin configuration.

Structural findings well agree with vibrational results. In the ligands, the increase of CO and CS bond and decrease of CN distances related to the amide-like or thioamide-like nature of these moieties, should be reflected on coordination by a shift of related vibration. Accordingly in the Me₂pipto case $\nu(\text{CO})$ and $\nu(\text{CN})$ stretching vibrations are observed for **1–4** in the range 1657–1638 cm^{−1}, and 1573–1553 cm^{−1} respectively with respect to the corresponding ones in the free ligand (1669 and 1527 cm^{−1}). In the Me₂pipdt case the $\nu(\text{CN})$ at 1500 cm^{−1} in the free ligand is found in the range 1548–1520 cm^{−1} for **5–7**. The CS vibration, being extensively coupled with other vibrations and thus difficult to be identified unambiguously, is not suitable to be used for similar correlation.

As far as the different kinds of polyiodides present in **6** and **7** Raman spectroscopy can help in complementing the structural information obtained by the X-ray data. The stretching frequency of solid I₂ [d(I–I) = 2.715 Å] falls near 180 cm^{−1}. For polyiodides containing a linear symmetrical I₃[−] ion, with interiodine distances elongated to 2.925 Å and describable with a three-center four electron covalent bond, the Raman active symmetrical stretching mode occurs near 110 cm^{−1}, while the antisymmetrical (140 cm^{−1}) and deformation (70 cm^{−1}) modes, active in the IR, can appear in the Raman only when I₃[−] become asymmetric due to solid state interactions. Higher polyiodides can be described as due to a combination of triiodides or iodides with I₂, as a consequence of a typical donor-acceptor interaction, which gives rise to a lowering of I₂ frequency, as a consequence of I–I elongation caused by the weak I[−]⋯I₂ interactions. The FT-Raman spectrum of compound **7** is reported in Figure 6. It shows two peaks at 108 and 147 cm^{−1}, in agreement with the presence of a symmetric I₃[−] and a largely elongated I₂, respectively, which may be due to interactions with two iodides (formally a I₄^{2−}).²⁸ As far as compound **6** is concerned, it underwent decomposition when submitted to the laser excitation source and no FT-Raman spectra could be obtained.

Magnetic properties

The molar magnetic susceptibility (χ_m) is shown for **1–5** in Figure 7 as a function of temperature. The behaviour may be described

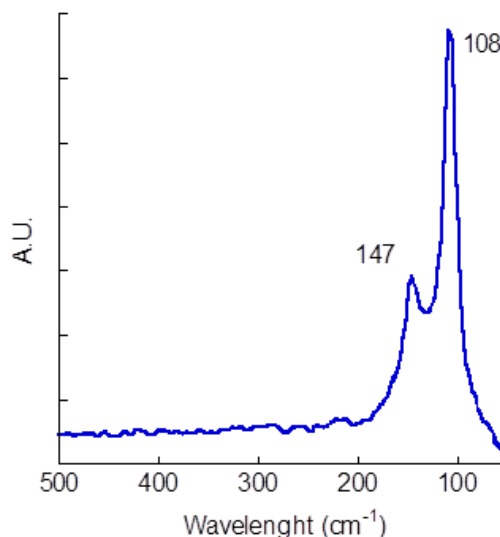


Figure 6. FT-Raman spectrum of **7**.

by a Curie-Weiss law:²⁹

$$\chi_m(T) = C/(T-\theta) \quad (1)$$

with $C = Np^2\beta^2/(3k)$, where N is the number of magnetic ions in a mole, p is the effective number of Bohr's magnetons, β is the Bohr magneton, k is the Boltzmann constant and θ is the Curie-Weiss constant. The values of p of the samples **1** and **4** (6.1 and 5.9, respectively) are similar to the reference value 5.9 for high spin Fe^{III}; the p value of sample **2** (5.5) is similar to the reference value 5.4 for high spin Fe^{II}.²⁹ The value $p = 4.2$ of sample **3** is compatible with high spin Co^{II} ion (reference value 4.8).²⁹ Samples **5–7** are diamagnetic in agreement with Fe^{II} and Co^{III} ions in low spin configuration.

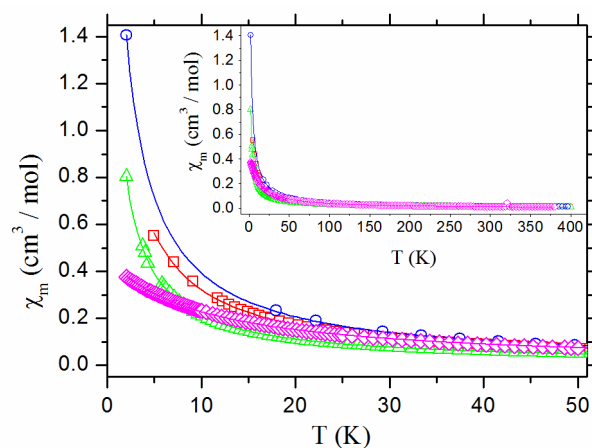


Figure 7. Molar magnetic susceptibility vs. temperature of samples **1** (red squares), **2** (black circles), **3** (blue lozenges) and **4** (green triangles) are reported in detail in the range 2–50 K. The experimental data are shown as empty circles, while the continuous line shows the best fit. The inset shows the data in the whole range of measurement (2–400 K).

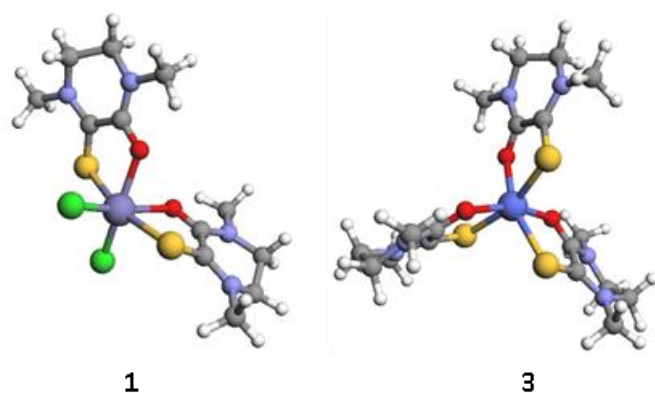


Figure 8. Calculated structures optimized at B3LYP/6-31G(d) level of theory.

In conclusion, as far as the magnetic properties are concerned, iron and cobalt complexes with the Me₂pipto ligand/s give rise to high spin derivatives, while those with Me₂pipdt to low-spin ones. Regarding the oxidation state of the metal, in the Me₂pipdt homoleptic complexes, the cobalt ion reaches the 3+ state; instead in the corresponding Me₂pipto case both iron and cobalt are found in the 2+ state. The 3+ oxidation state for iron is reached in the heteroleptic complexes **1** and **4**, where the presence of negatively charged ligands (Cl⁻ and NCS⁻) may help in stabilizing the high charge. A qualitative description of bonding according to the ligand field theory for metals in an octahedral geometry can explain the observed results. The higher σ -donor and the π -acceptor capabilities of S,S' donor (see Figure S1) allow the related orbitals to interact with 3d metal orbitals inducing e_g destabilization and t_{2g} stabilization through the π -back-donation from the metal orbitals to the LUMO of the ligand. The resulting high energy gap between e_g and t_{2g} will favor the low-spin state and the easy removal of one electron from the high lying e_g orbital as found in iron(II) and cobalt(III) **5-7** derivatives. In the S,O case the introduction of one oxygen atom lowers both σ -donor and the π -acceptor capability of the ligand in such a way that e_g destabilization and t_{2g} stabilization are weaker. This results in a lower energy gap favoring high spin state for iron(II) in **1** and cobalt(II) which maintains its oxidation state in **3**. Theoretical calculations, (see below) have been performed to predict the ground state of some iron and cobalt complexes.

30 Computational studies

DFT calculations for the complexes **2** and **5**, already reported in a short communication,⁸ have been performed by employing OLYP functional to optimize the geometries of these iron(II) high and low spin complexes **2** (S,O) and **5** (S,S') for the singlet ($S = 0$) and quintet ($S = 2$) states. From a comparison of the experimental and calculated bond distances, the preferred ground states for complexes were respectively the $S = 2$ and $S = 0$, with an energy preference for the $S = 2$ state over the $S = 0$ one of 60.14 kJ mol⁻¹ for **2**, and for the $S = 0$ state over the $S = 2$ one of 31.88 kJ mol⁻¹ for **5**.

Results from analogous calculations for **1** and **3** are reported here. The ground state geometries, optimized in the gas-phase at the B3LYP/6-31G(d) level of theory, are shown in Figure 8. Experimental and calculated structures are in good agreement for compound **1** (see Figure S7). The differences in the bond

distances are lower than 0.09 Å, except for Fe-S12 (~0.13 Å), and in angles are around 4° with a highpoint of 10° (Cl-Fe-Cl) and a minimum of 1° for the O-Fe-O angle (Table S1). B3LYP geometry optimization has been done for the complex **1** also in the low spin configuration. As predictable, the lengths of the bonds involving the metal center are shorter than those found for the sextet state, except for the Fe-Cl bonds that are very similar (Table S2). However, the comparison with the X-ray experimental distances, does not allow to establish clearly which configuration is preferred. Further calculations, both in the high and low spin state, have thus been performed employing OLYP, a pure DFT functional which has shown to work well to predict the ground state of **2** and **5** as well other iron complexes (Table S2).³⁰ Similarly to results obtained with B3LYP, the Fe-S and Fe-O distances are shorter in the LS spin state also with results obtained with OLYP. Thus, since the comparison of the structural data do not allow to univocally pick out the preferred configuration, the calculated energies have been employed for this purpose: both functionals evaluated the $S = 5/2$ state as the most stable by 99.85 and 94.45 kJmol⁻¹ for B3LYP and OLYP, respectively (Table S5). Similarly for the complex [Co(Me₂pipto)₃](BF₄)₂ both functionals predict the quartet state as more stable than the doublet one, by 61.72 kJmol⁻¹ for B3LYP and 7.57 kJmol⁻¹ for OLYP (Table S6) in agreement with the magnetic measurements.

Conclusions

The coordination of S,O (Me₂pipto) and S,S' (Me₂pipdt) chelating donor ligands to iron and cobalt ions affords a variety of metal complexes which differ for coordination, metal oxidation state, and spin state. Substituting one oxygen atom to the sulphur one in the chelating C2S2 moiety lead to the formation of iron and cobalt complexes which in homoleptic [M(Me₂pipto)₃]²⁺ are both in the oxidation state 2+ and high spin state (**2** and **3**), while in the corresponding Me₂pipdt homoleptic complexes (**5**, **6** and **7**), while iron is still found in the state 2+ and the cobalt ion reaches the 3+ state, but both are in the low spin state. Computational studies have been performed at DFT level using B3LYP and OLYP as functional and the most stable spin state configurations predicted for both of them, are in accordance with the magnetic measurements results.

As whole, the obtained results can be explained by taking into account the higher σ -donor and the π -acceptor capability of S,S' donor ligand with respect to the S,O one, affording increased overlap between the ligand frontier orbitals and the metal orbitals and thus increasing the e_g - t_{2g} energy separation. The tunability of the properties shown by complexes on tuning O/S atoms in Me₂pipto, and Me₂pipdt suggests switchable materials may be affordable.

95 Acknowledgements

L. P. gratefully acknowledges Sardinia Regional Government for the financial support (P.O.R. Sardegna F.S.E. Operational Programme of the Autonomous Region of Sardinia, European Social Fund 2007-2013-Axis IV Human Resources, Objective I.3, Line of Activity I.3.1 "Avviso di chiamata per il finanziamento di

Assegni di Ricerca”). M.L.M. and D.E. acknowledge Regione Autonoma della Sardegna, L.R. 7-8-2007, Bando 2009, CRP-17453 Project “Nano Materiali Multifunzionali per Applicazioni nell’Elettronica Molecolare”, Fondazione Banco di Sardegna and 5 INSTM.

Notes and references

^a Dipartimento di Ingegneria Meccanica Chimica e dei Materiali, Università di Cagliari, via Marengo 2, 109123, Cagliari, Italy. E-mail:

^b pilialu@unica.it

^b Dipartimento di Scienze Chimiche e Geologiche, Università di Cagliari, S.S. 554-Bivio per Sestu, 109042 Monserrato-Cagliari, Italy. E-mail:

^c deplano@unica.it

^c Dipartimento di Fisica, Università di Cagliari, S.P. Monserrato - Sestu Km 0.700, 109042 Monserrato (CA), Italy.

^d Dipartimento di Chimica, Università di Parma, Parco Area delle Scienze 17A, I43124 Parma, Italy.

† Electronic Supplementary Information (ESI) available: Figure S1, Drawings and energies of ligands’ Orbitals; Figures S2-S6 crystal packing 20 of **1** and **4-7**; Figure S7 experimental and calculated structures of **1** and Tables S1-S6 computational results. See DOI: 10.1039/b000000x/

- R. G. Pearson, *J. Am. Chem. Soc.*, 1963, **85**, 3533.
- (a) M. Kato, K. Unoura, T. Takayanagi, Y. Ikeda, T. Fujihara and A. Nagasawa, *Inorg. Chem.*, 2013, **52**, 13375; (b) A. Tomita and M. Sano, *Inorg. Chem.*, 1994, **33**, 5825; (c) A. Yeh, N. Scott and H. Taube, *Inorg. Chem.*, 1982, **21**, 2542.
- (a) G. H. Spikes, E. Bill, T. Weyhermüller and K. Wieghardt, *Angew. Chem., Int. Ed.*, 2008, **47**, 2973; (b) C. G. Pierpont and C. W. Lange, *Prog. Inorg. Chem.*, 1994, **41**, 331; (c) R. Eisenberg and H. B. Gray, *Inorg. Chem.*, 2011, **50**, 9741; (d) S. Sproules and K. Wieghardt, *Coord. Chem. Rev.*, 2010, **254**, 1358; (e) P. Deplano, L. Pilia, D. Espa, M. L. Mercuri and A. Serpe, *Coord. Chem. Rev.*, 2010, **254**, 1434; (f) F. Ehret, M. Bubrin, R. Hübner, D. Schweinfurth, I. Hartenbach, S. Zális and W. Kaim, *Inorg. Chem.*, 2012, **51**, 6237.
- (a) F. Bigoli, P. Deplano, M. L. Mercuri, M. A. Pellinghelli, G. Pintus, A. Serpe and E. F. Trogu, *J. Am. Chem. Soc.*, 2001, **123**, 1788; (b) A. Serpe, F. Bigoli, M. C. Cabras, P. Fornasiero, M. Graziani, M. L. Mercuri, T. Montini, L. Pilia, E. F. Trogu and P. Deplano, *Chem. Comm.*, 2005, 1040; (c) A. Serpe, F. Artizzu, M. L. Mercuri, L. Pilia and P. Deplano, *Coord. Chem. Rev.*, 2008, **252**, 1200; (d) A. Serpe, F. Artizzu, L. Marchiò, M. L. Mercuri, L. Pilia and P. Deplano, *Cryst. Growth Des.*, 2011, **11**, 1278.
- (a) F. Bigoli, C.-T. Chen, W.-C. Wu, P. Deplano, M. L. Mercuri, M. A. Pellinghelli, L. Pilia, G. Pintus, A. Serpe and E. F. Trogu, *Chem. Commun.*, 2001, 2246; (b) F. Bigoli, P. Deplano, M. L. Mercuri, M. A. Pellinghelli, L. Pilia, G. Pintus, A. Serpe and E. F. Trogu, *Inorg. Chem.*, 2002, **41**, 5241; (c) P. Deplano, M. L. Mercuri, L. Marchiò, L. Pilia, M. Salidu, A. Serpe and E. Tronci, *Inorg. Chim. Acta*, 2004, **357**, 1608; (d) P. Deplano, M. L. Mercuri, L. Marchiò, L. Pilia, M. Salidu, A. Serpe, F. Congiu and S. Sanna, *Eur. J. Inorg. Chem.*, 2005, 1829; (e) F. Bigoli, P. Deplano, M. L. Mercuri, L. Marchiò, L. Pilia, M. Salidu, A. Serpe, F. Congiu and S. Sanna, *Chem. Phys. Letters*, 2006, **421**, 361.
- (a) S. Curreli, P. Deplano, C. Faulmann, A. Ienco, C. Mealli, M. L. Mercuri, L. Pilia, G. Pintus, A. Serpe and E. F. Trogu, *Inorg. Chem.* 2004, **43**, 5069; (b) P. Deplano, M. L. Mercuri, A. Serpe and L. Pilia, chapter 16 in the book *The Chemistry of Metal Enolates*, (Ed: J. Zabicky), John Wiley & Sons, Chichester, 2009; (c) D. Espa, L. Pilia, L. Marchiò, M. Pizzotti, N. Robertson, F. Tessore, M. L. Mercuri, A. Serpe and P. Deplano, *Dalton Trans.*, 2012, **41**, 12106; (d) D. Espa, L. Pilia, L. Marchiò, F. Artizzu, A. Serpe, M. L. Mercuri, D. Simão, M. Almeida, M. Pizzotti, F. Tessore and P. Deplano, *Dalton Trans.*, 2012, **41**, 3485; (e) L. Pilia, D. Espa, A. Barsella, A. Fort, C. Makedonas, L. Marchiò, M. L. Mercuri, A. Serpe, C. A. Mitsopoulou and P. Deplano, *Inorg. Chem.*, 2011, **50**, 10015; (f) D. Espa, L. Pilia, L. Marchiò, M. L. Mercuri, A. Serpe, A. Barsella, A. Fort, S. J. Dalglish, N. Robertson and P. Deplano, *Inorg. Chem.*, 2011, **50**, 2058; (g) F. Frei, A. Rondi, D. Espa, M. L. Mercuri, L. Pilia, A. Serpe, A. Odeh, F. Van Mourik, M. Chergui, T. Feurer, P. Deplano, A. Vlček, Jr. and A. Cannizzo, *Dalton Trans.*, 2014, **43**, 17666.
- V. N. Nemykin, J. G. Olsen, E. Perera and P. Basu, *Inorg. Chem.* 2006, **45**, 3557.
- L. Pilia, F. Artizzu, D. Espa, L. Marchiò, M. L. Mercuri, A. Serpe and P. Deplano, *Dalton Trans.*, 2010, **39**, 8139.
- R. Isaksson, T. Liljefors and J. Sandstrom, *J. Chem. Res., Mimirprint*, 1981, 664.
- SMART (control) and SAINT (integration) software for CCD systems, Bruker AXS, Madison, WI, USA, 1994.
- (a) N. Walker and D. Stuart, *Acta Crystallogr., Sect. A* 1983, **39**, 158; (b) F. Uguzzoli, *Comput. Chem.* 1987, **11**, 109.
- Area-Detector Absorption Correction, SADABS; Bruker AXS Inc., Madison, WI, USA, 2001.
- A. Altomare, M. C. Burla, M. Camalli, G. L. Casciarano, C. Giacovazzo, A. Guagliardi, A. G. G. Moliterni, G. Polidori and R. Spagna, *J. Appl. Crystallogr.* 1999, **32**, 115.
- M. C. Burla, R. Caliendo, M. Camalli, B. Carrozzini, G. L. Casciarano, L. De Caro, C. Giacovazzo, G. Polidori and R. Spagna, *J. Appl. Crystallogr.* 2005, **38**, 381.
- G. M. Sheldrick, SHELX97. Programs for Crystal Structure Analysis 1997 (Release 97-2), University of Göttingen, Germany.
- L. J. Farrugia, WinGX and ORTEP for Windows: an update. *J. Appl. Crystallogr.* 2012, **45**, 849.
- C. F. Macrae, I. J. Bruno, J. A. Chisholm, P. R. Edgington, P. McCabe, E. Pidcock, L. Rodriguez-Monge, R. Taylor, J. van de Streek and P. A. Wood, *J. Appl. Crystallogr.* 2008, **41**, 466.
- R. G. Parr and W. Yang, *Density Functional Theory of Atoms and Molecules*, Oxford University Press: Oxford, 1989.
- Gaussian 09, Revision D.01, M. J. Frisch, G. W. Trucks, H. B. Schlegel, G. E. Scuseria, M. A. Robb, J. R. Cheeseman, G. Scalmani, V. Barone, B. Mennucci, G. A. Petersson, H. Nakatsuji, M. Caricato, X. Li, H. P. Hratchian, A. F. Izmaylov, J. Bloino, G. Zheng, J. L. Sonnenberg, M. Hada, M. Ehara, K. Toyota, R. Fukuda, J. Hasegawa, M. Ishida, T. Nakajima, Y. Honda, O. Kitao, H. Nakai, T. Vreven, J. A. Jr. Montgomery, J. E. Peralta, F. Ogliaro, M. Bearpark, J. J. Heyd, E. Brothers, K. N. Kudin, V. N. Staroverov, R. Kobayashi, J. Normand, K. Raghavachari, A. Rendell, J. C. Burant, S. S. Iyengar, J. Tomasi, M. Cossi, N. Rega, N. J. Millam, M. Klene, J. E. Knox, J. B. Cross, V. Bakken, C. Adamo, J. Jaramillo, R. Gomperts, R. E. Stratmann, O. Yazyev, A. J. Austin, R. Cammi, C. Pomelli, J. W. Ochterski, R. L. Martin, K. Morokuma, V. G. Zakrzewski, G. A. Voth, P. Salvador, J. J. Dannenberg, S. Dapprich, A. D. Daniels, Ö. Farkas, J.B. Foresman, J. V. Ortiz, J. Cioslowski and D. J. Fox, Gaussian, Inc., Wallingford CT, 2009.
- A. D. Becke, *J. Chem. Phys.* 1993, **98**, 5648.
- C. Lee, W. Yang and R. G. Parr, *Phys. Rev. B* 1988, **37**, 785.
- R. Ditchfield, W. J. Hehre and J. A. Pople, *J. Chem. Phys.* 1971, **54**, 724.
- V. A. Rassolov, M. A. Ratner, J. A. Pople, P. C. Redfern and L. A. Curtiss, *J. Comp. Chem.* 2001, **22**, 976.
- N. C. Handy and A. J. Cohen, *Mol. Phys.* 2001, **99**, 403.
- M.A. Thompson, ArgusLab 4.0.1; Planaria Software LLC: Seattle, WA, <http://www.arguslab.com/arguslab.com/ArgusLab.html/>.
- R. Krishnan, J. S. Binkley, R. Seeger and J. A. Pople, *J. Chem. Phys.* 1980, **72**, 650.
- A. D. McLean and G. S. Chandler, *J. Chem. Phys.* 1980, **72**, 5639.
- P. Deplano, J. R. Ferraro, M. L. Mercuri and E. F. Trogu, *Coord. Chem. Rev.* 1999, **188**, 71.
- A.H. Morrish, *The Physical Principles of Magnetism*, IEEE Press, New York, 2001.
- (a) M. Swart, *J. Chem. Theory Comput.* 2008, **4**, 2057; (b) J. Conradie and A. Ghosh, *J. Chem. Theory Comput.* 2007, **3**, 689.